Hindawi Publishing Corporation
International Journal of Metals
Volume 2015, Article ID 632021, 13 pages
http://dx.doi.org/10.1155/2015/632021

Research Article

Effects of Moulding Sand Permeability and Pouring Temperatures on Properties of Cast 6061 Aluminium Alloy

Olawale Olarewaju Ajibola,[1,2] Daniel Toyin Oloruntoba,[1] and Benjamin O. Adewuyi[1]

[1]*Metallurgical and Materials Engineering Department, Federal University of Technology Akure, Akure 340252, Nigeria*
[2]*Materials and Metallurgical Engineering Department, Federal University Oye Ekiti, Oye Ekiti 371104, Nigeria*

Correspondence should be addressed to Olawale Olarewaju Ajibola; olawale.ajibola@fuoye.edu.ng

Received 26 May 2015; Revised 2 September 2015; Accepted 14 September 2015

Academic Editor: Manoj Gupta

Effects of moulding sand permeabilities prepared from the combinations of four proportions of coarse and fine particle size mixtures and pouring temperatures varied from 700, 750, and 800 (±10°C) were studied on the hardness, porosity, strength, and microstructure of cast aluminium pistons used in hydraulic brake master cylinder. Three sand moulds were prepared from each of the 80 : 20, 60 : 40, 40 : 60, and 20 : 80 ratios. The surfaces and microstructures of cast samples were examined using high resolution microscopic camera, metallurgical microscope with digital camera, and scanning electron microscope with EDX facilities. The best of the metallurgical properties were obtained from the combination of 80 : 20 coarse-fine sand ratio and 750 ± 10°C pouring temperature using as MgFeSi inoculant. An 8 : 25 ratio of coarse to fine grained eutectic aluminium alloy was obtained with enhanced metallographic properties. The cast alloy poured at 750 ± 1°C has a large number of fine grain formations assuming broom-resembling structures as shown in the 100 μm size SEM image.

1. Introduction

Aluminium recycling industries are growing globally at very alarming rate. In Nigeria, the entrepreneurship challenges and opportunities that go along with this trend are also vast [1]. Hence, the research and development affect many facets such as the aluminium foundry, materials design for various fields of applications such as automobile and automotive industries [2]. The metallurgical properties of metal alloys are controlled by many factors such as the chemical composition, microstructure, processing methods such as casting [3], extrusion, and postproduction treatment such as surface deposition and heat treatment [4–6].

These mentioned factors definitely affect the microstructures of the product and consequently determine the behaviour of the cast under the stipulated service [7]. In order to improve the quality of the aluminium alloy piston used in the hydraulic brake master cylinder, a controlled casting technique involving melting and pouring temperature, selective combination of moulding sand permeability and finally the solidification and cooling process will have great deal on the microstructure, mechanical strength, hardness, and hence the wear resistance of the product. The sand particle size distribution controls the mould permeability which is the amount of air that can be trapped through the sand in the mould. It was reported that the coarse particle size results in high permeability while fine particles give low permeability of moulding sand [8].

Dissolved gases increase the chances of pores formation thereby increasing the porosity in the metal cast whereas the enclosure or inclusion of the surface energy effect makes it difficult, which likely need negative pressure to form empty spaces (voids). Dissolved gases in liquid alloy cause porosity because the solubility of gases in liquid metals usually exceeds the solubility in the solid.

It is in most cases required that the cast alloy material should be impervious to gases and liquids. The porosity is higher when more pores are contained in the cast. Hence, there is tendency of heat loss by convection and the leakages of liquid through the pores of the metal cast. In some refractory metals, thermal shock depends on porosity of the material. The porous materials (compressed powder metals)

Table 1: Particle size (μm) distribution of moulding sand.

	Coarse sand						Fine sand					
Sieve range (μm)	+4750	−4750 +2360	−2360 +1180	−1180 +850	−850 +600	−600 +425	−425 +300	−300 +212	−212 +180	−180 +150	−150 +75	−75
% distribution	0.82	1.55	3.57	8.61	9.01	9.75	13.81	14.03	13.21	11.86	8.05	5.72

Table 2: Pouring temperatures and mixing ratios of coarse and fine moulding sand.

Temperature ˚C	Mixing ratios coarse (−1180 +300 μm) and fine (−300 +75 μm) moulding sand			
	Set 1	Set 2	Set 3	Set 4
700	80 : 20	60 : 40	40 : 60	20 : 80
750	80 : 20	60 : 40	40 : 60	20 : 80
800	80 : 20	60 : 40	40 : 60	20 : 80

have higher resistance to spall than the highly compacted shapes. Therefore, depending on the application, there should be a balance between the porosity and compactness of the material.

Hence, the effects of sand permeability via particle sizes of the moulding sand and variation of pouring temperatures on the properties (strength, hardness, and porosity) of cast aluminium alloy (AA6061) were studied in this report.

2. Materials

The materials used in the experiment include the foundry moulding sands (coarse and fine), 1000 kg of aluminium alloy (AA6061) scrap sourced from the brake master cylinder pistons, and powdered magnesium ferrosilicon inoculant.

3. Method

3.1. Procedure for Sand Cast Specimen. The moulding sand was prepared from different proportions of coarse and fine sand particle sizes. Table 1 shows the sand particles size distribution of moulding sand used. Three sets of moulds were prepared from each of the 80 : 20, 60 : 40, 40 : 60, and 20 : 80 ratios of coarse (+4750 +300 μm) and fine (−300 −75 μm) moulding sand particle size mixtures (Table 2 and Figures 1-2). The sand was properly rammed with adequate vent holes. The moulds were left to dry at room temperature (27˚C).

Aluminium scrap was charged into the melting crucible and fired. The molten Al alloy was held at three pouring temperature ranges (700 ± 10˚C, 750 ± 10˚C, and 800 ± 10˚C). 17 g of powdered magnesium ferrosilicon inoculant was added per 1 kg mass of molten metal in the melting pot and before casting [3]. The moulding flasks were preheated before the casting process. To study the effect of variation in the moulding sand permeability and pouring temperatures, twelve specimens were cast at the three pouring temperatures (700 ± 10˚C, 750 ± 10˚C, and 800 ± 10˚C) using the prepared ratios of coarse-fine moulds (80 : 20, 60 : 40, 40 : 60, and 20 : 80). The method used for the determination of the moulding sand permeability has been described by Jimoh et al. [9].

The aluminium cast was left to solidify and cool to room temperature in the mould. The cast samples were removed from the mould and fettled. It is lightly machined on the lathe to rod of 300 mm long by 30 mm diameter (Figure 3(a)) from which samples were cut for hardness test and tensile strength test (Figure 3(b)). The cross cut section was also examined under microscope. The cast samples from each of the sand mould were designated as TS11–TS14; TS21–TS24; and TS31–TS34 for each set of cast Al alloy poured at 700 ± 10˚C, 750 ± 10˚C, and 800 ± 10˚C, respectively (Figures 3–9).

To determine the porosity of the cast samples, 25 mm × 25 mm × 25 mm cube size test samples were cut from the core of the cylindrical shape cast Al alloy to be tested. The test samples were cleaned from dust and other particles adhering to the surfaces and fired at 110˚C in oven to a dry weight (D). The dried specimen is placed in the vacuum desiccator which is then evacuated to a pressure of 2.5 mm Hg. The specimen is immersed in liquid paraffin (boiling above 200˚C). The test samples were soaked in the liquid under reduced pressure for 10 hours suspended by a sling thread and were weighed (S) while still suspended in immersion liquid. The test specimen is then lifted up slowly from the immersion liquid by means of the sling thread liquid, and drops appearing on the surface are removed by lightly contacting with a piece of blotting ensuring that it does not make physical contact with the specimen surface itself. The soaked specimen is latter weighed (W) while keeping it suspended in air. The apparent porosity (P) is then calculated as follows:

$$P = \left(\frac{W - D}{W - S}\right) \times 100\,(\%)\,. \tag{1}$$

3.2. Chemical and Physical Characterisation of Scrap and Cast Samples. The hardness tests of aluminium alloy samples (the scrap and cast Al alloy) were also determined using Brinell Hardness Testing Machine. The test was conducted by pressing a tungsten carbide sphere 10 mm in diameter into the test plate surface for 10 seconds with a load of 1500 kg, and then the diameter of the resulting depression is measured. An average of four BHN tests was carried out over an area of the specimen surface. The BHN is calculated using (2) and average HBN values from the result are presented in Figures 3(a) and 3(b):

$$\text{BHN} = \frac{F}{\left[\pi D/2\left(D - \sqrt{D^2 - D_i^{\,2}}\right)\right]}, \tag{2}$$

where BHN is the Brinell hardness number, F is imposed load in kg, D is diameter of the spherical indenter in mm, and D_i is diameter of the resulting indenter impression in mm.

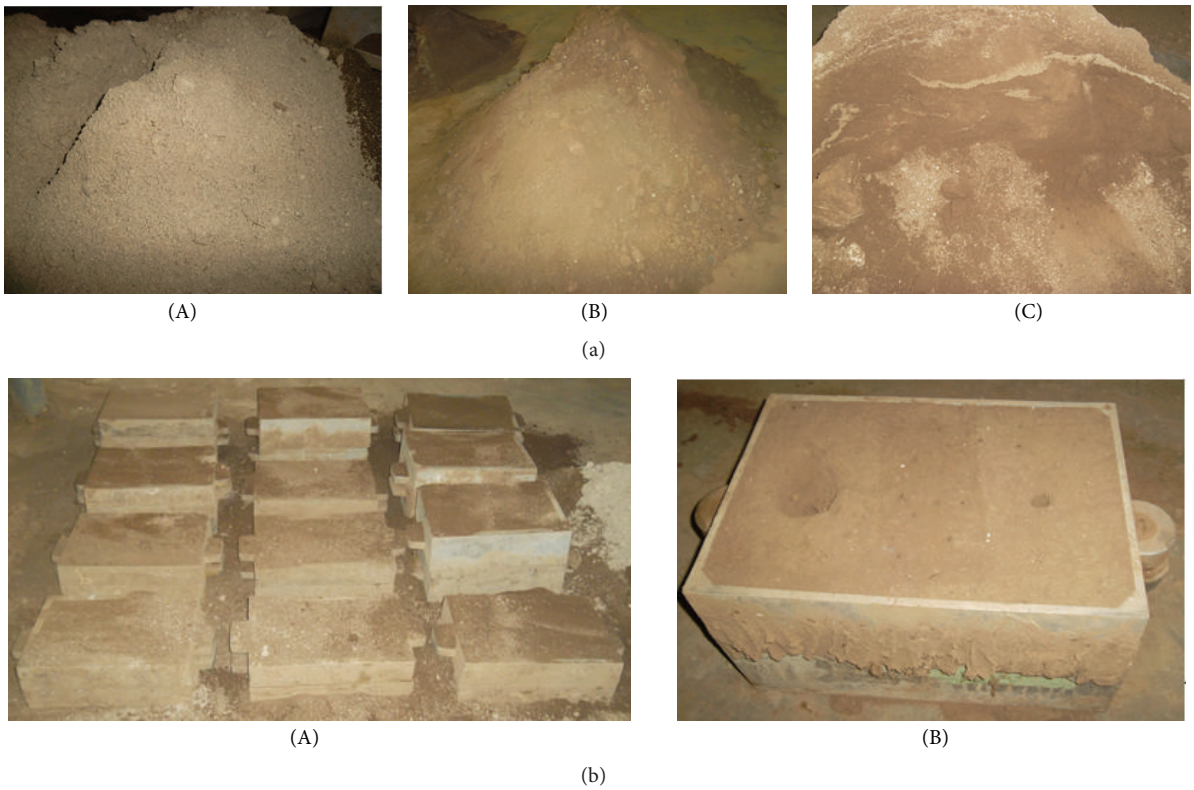

Figure 1: (a) Photographs showing (A) coarse size (+4750 +300 μm), (B) fine size (−300 −75 μm), and (C) moulding sand mixtures. (b) Photographs showing (A, B) matrix of twelve moulding flasks.

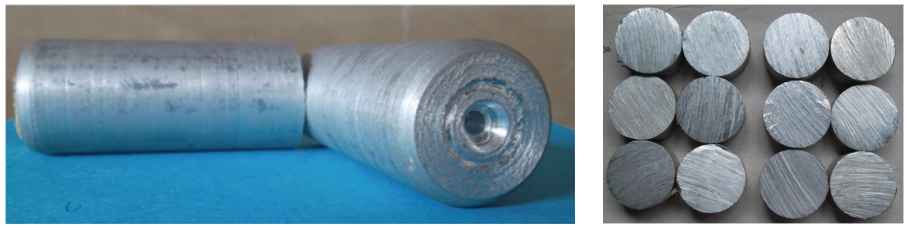

Figure 2: Photographs showing (a) machined cast aluminium alloy and (b) cast specimens used for photomicroscopy and SEM analyses.

The grain sizes of the microscopic particles of the purchased piston and cast aluminium alloy samples were determined using XRD. The powder of each sample was produced for XRD study under higher resolution X-ray using X-Ray Minidiffractometer MD-10 model with digital facilities. Each of the peak values in the diffractograms was interpreted by comparing the values with the standard values in the database of compounds under this radiation using the "search and match" technique.

The surfaces of cast samples were examined under high resolution microscopic camera using Samsung ST65-HD5X-14.2 model. Microstructures of the scrap and cast samples were examined under higher resolution metallurgical microscope with digital camera (Accu-Scope microscope model) in the laboratory at ×800 magnification.

The cast samples were further characterised by Atomic Absorption Spectroscopy (AAS-Thermo series 2000 model), X-Ray diffraction (XRD) (Minidiffractometer MD-10 model with digital facilities), and Scanning Electron Microscopy (SEM) and Energy Dispersive X-Ray (EDX) analyses (Jeol JSM-7600F Field Emission). The macrophotographs, micrographs, diffractograms, SEM/EDX spectra line, and AAS data generated were used to interpret the results.

4. Results and Discussions

The chemical compositions of scrap and cast samples are presented in Table 3. The chemical analysis by AAS shows that scrap aluminium alloy contains 98.665% Al as matrix and the following alloying elements: 0.686% Si, 0.403% Mg, 0.001%

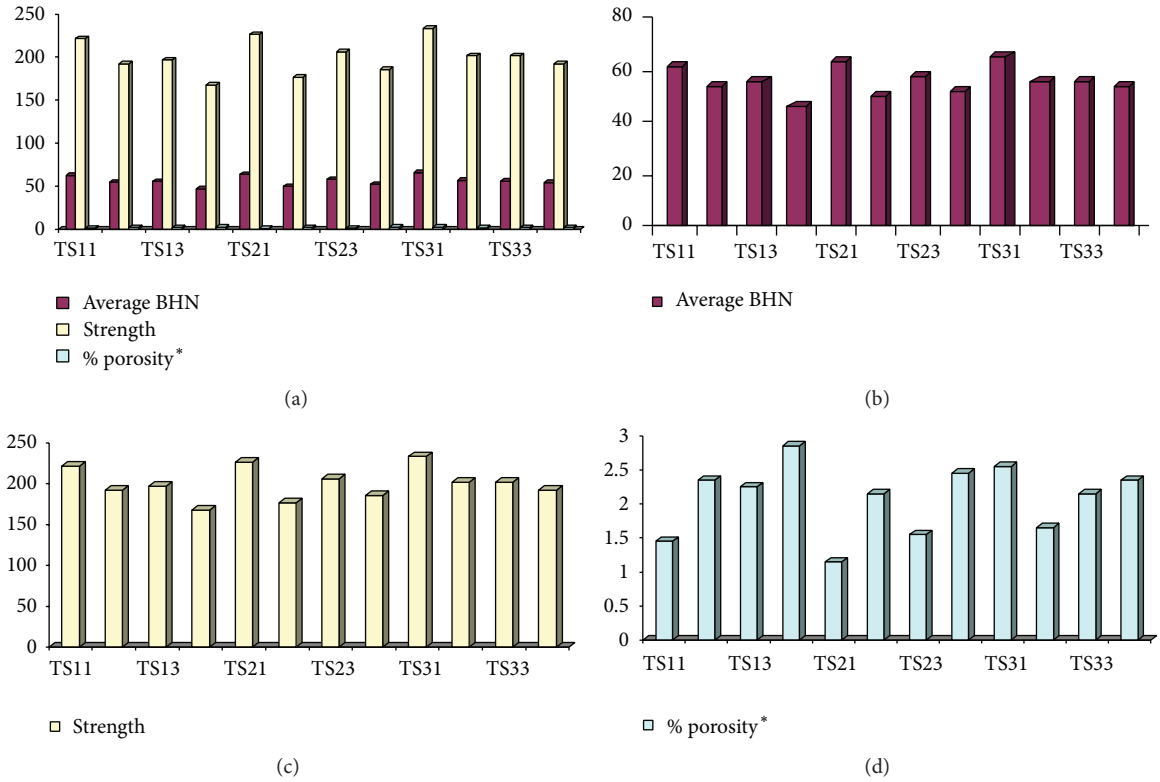

Figure 3: (a) Properties of cast aluminium alloy (TS11–TS34) at varying pouring temperatures (700, 750, and 800°C) and different moulding sand ratios. (b) BHN of cast aluminium alloy (TS11–TS34) at varying pouring temperatures (700, 750, and 800°C) and different moulding sand ratios. (c) Strength of cast aluminium alloy (TS11–TS34) at varying pouring temperatures (700, 750, and 800°C) and different moulding sand ratios. (d) Porosity of cast aluminium alloy (TS11-TS34) at varying pouring temperatures (700, 750, and 800°C) and different moulding sand ratios.

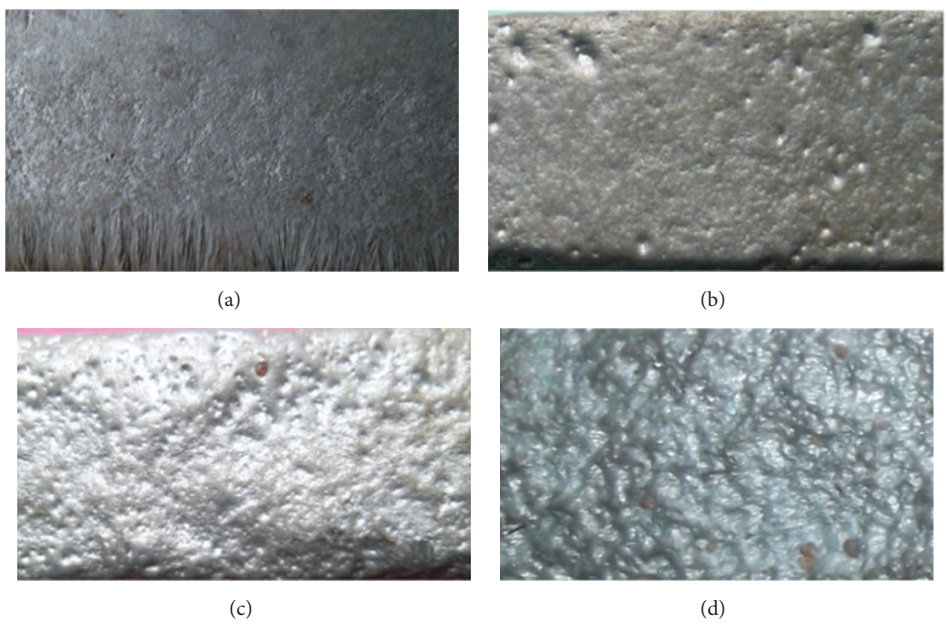

Figure 4: Surfaces of as-cast AA6061 aluminium alloy (TS11–TS14) at 700 ± 10°C pouring temperature at different moulding sand mixing ratios (a) 80 : 20, (b) 60 : 40, (c) 40 : 60, and (d) 20 : 80 (×10 mag.).

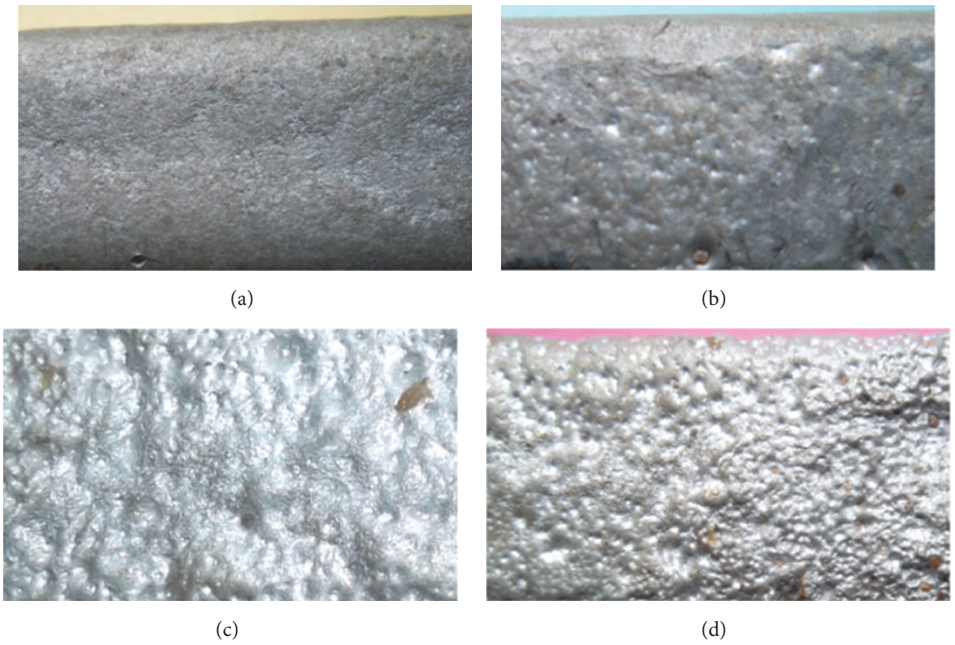

(a) (b) (c) (d)

Figure 5: Surfaces of as-cast AA6061 aluminium alloy (TS21–TS24) at 750 ± 10°C pouring temperature at different moulding sand mixing ratios (a) 80 : 20, (b) 60 : 40, (c) 40 : 60, and (d) 20 : 80 (×10 mag.).

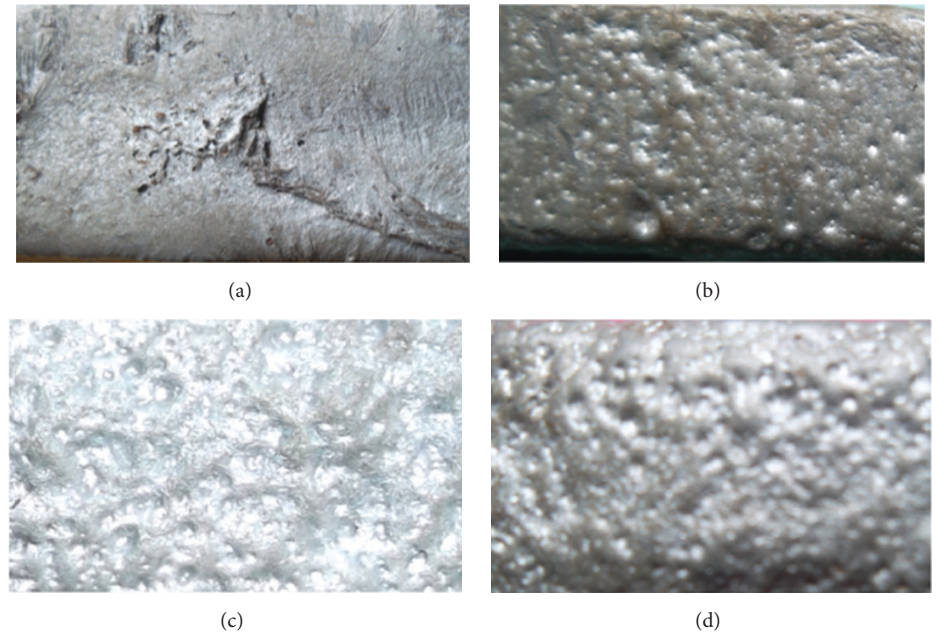

(a) (b) (c) (d)

Figure 6: Surfaces of as-cast AA6061 aluminium alloy (TS31–TS34) at 800 ± 10°C pouring temperature at different moulding sand mixing ratios (a) 80 : 20, (b) 60 : 40, (c) 40 : 60, and (d) 20 : 80 (×10 mag.).

Cu, 0.001% Zn, 0.001% Ti, 0.001% Mn, 0.001% Cr, and 0.232% Fe.

4.1. Influence of Sand Permeability and Pouring Temperatures on Cast Al Samples. The right casting process starts with the laying hold on the control of the chemistry of the melt. Casting aluminium alloy entails proper handling of the charge materials and the equipment. This ranges from the type of furnace and fuel, the melting pot, the selection of fluxing additives, and alloying elements.

The choice of the moulding sand permeability (moulding sand particles size mixing ratios) was used as one of the measures to obtain enhanced metallurgical properties (high HBN and eutectic microstructure) of the aluminium cast. The moulding sand was prepared from the combination of high coarse sand (+1180 +300 μm) to low fine (+300 +75 μm) sand

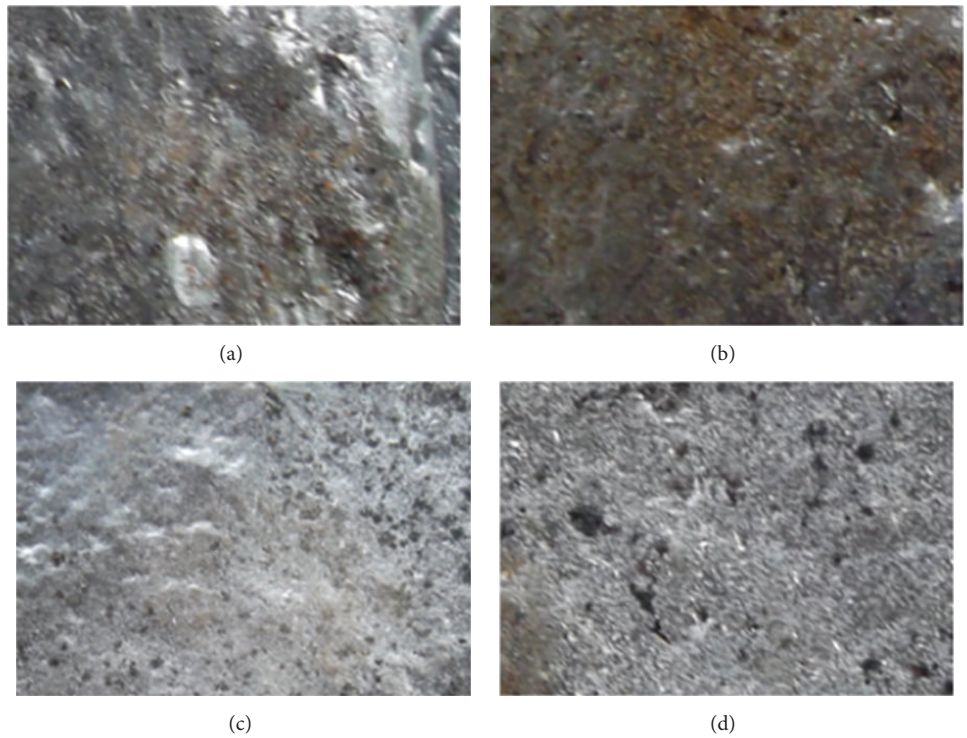

Figure 7: Enlarged micrographs showing porous cast aluminium alloy (TS11–TS14) at 700 ± 10°C pouring temperature at different moulding sand mixing ratios (a) 80 : 20, (b) 60 : 40, (c) 40 : 60, and (d) 20 : 80 (×100 mag.).

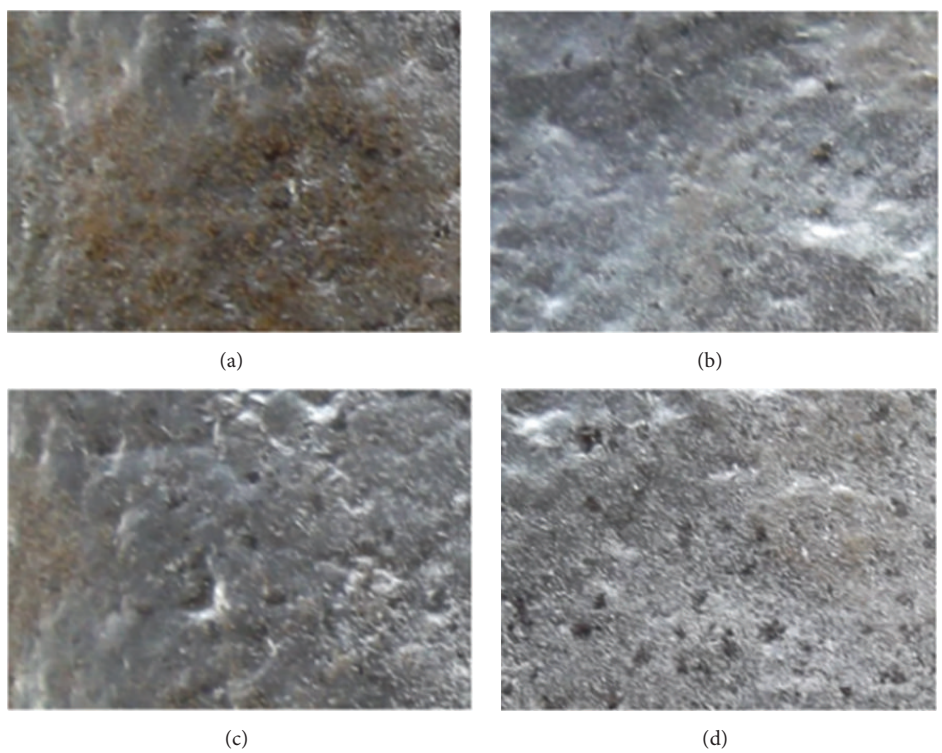

Figure 8: Enlarged micrographs showing porous cast aluminium alloy (TS21–TS24) at 750 ± 10°C pouring temperature at different moulding sand mixing ratios (a) 80 : 20, (b) 60 : 40, (c) 40 : 60, and (d) 20 : 80 (×100 mag.).

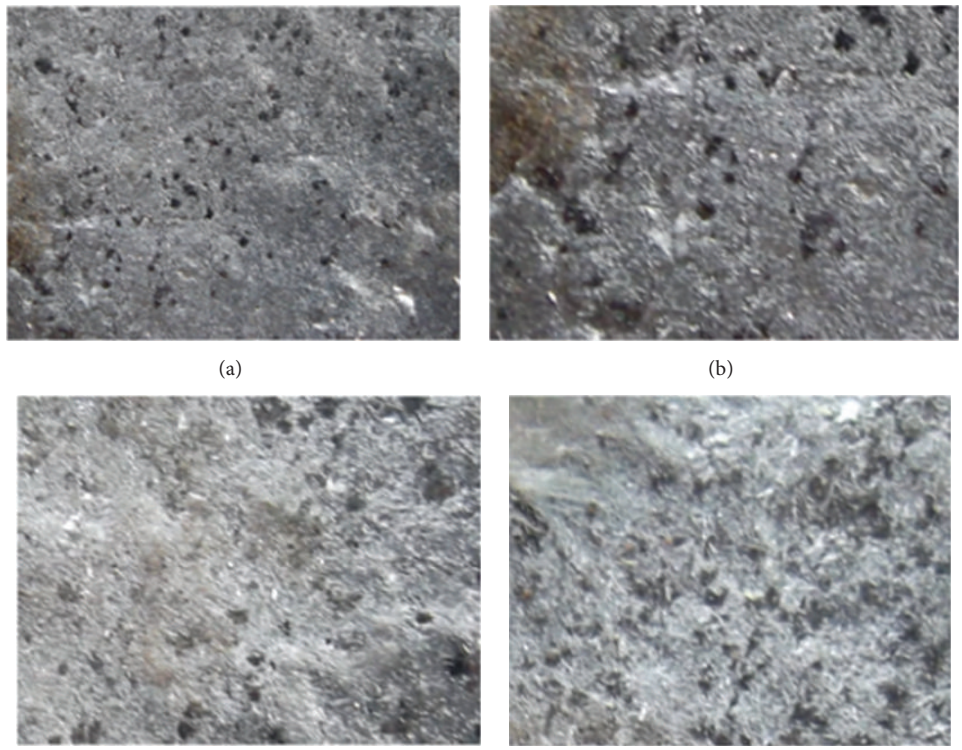

Figure 9: Enlarged micrographs showing porous cast aluminium alloy (TS31–TS34) at 800 ± 10°C pouring temperature at different moulding sand mixing ratios (a) 80 : 20, (b) 60 : 40, (c) 40 : 60, and (d) 20 : 80 (×100 mag.).

particle sizes to give moderately high permeability [10]. High permeability of moulding sand (80 : 20 coarse-fine ratios) allowed the escape of gases and air bubbles that would have entrapped in the mould thereby increasing the porosity of the cast piston.

The micrographs showing the microstructures of scrap and cast aluminium alloys poured at 700 ± 10°C, 750 ± 10°C, and 800 ± 10°C, respectively, are presented in Figures 4–14. The microstructural examinations revealed the microstructures of the alloys and compared the similarities and differences between the grain sizes and structures of scrap and cast samples (Figures 15-16), as influenced by the pouring temperature and the mixing ratio (permeability) of moulding sand.

Pouring an aluminium alloy at temperature above 690°C often gives enhanced metallurgical properties. The microstructure and phases of the aluminium cast were moderated and refined grains were obtained in agreement with Apelian [11]. The structure of cast sample poured at 700°C using 80 : 20 coarse-fine sand mixing ratio is characterised by fine grains as revealed by the SEM analysis with few pores and fine transitioned Al-Si eutectic (Figure 14) as compared with the scrap material [11].

As the pouring temperature of molten metal is higher, gas content will increase especially for molten aluminium. The choice of pouring at 750 ± 10°C was strategized to moderate the gas content in the molten aluminium alloy and to obtain eutectic structure of cast alloy [10].

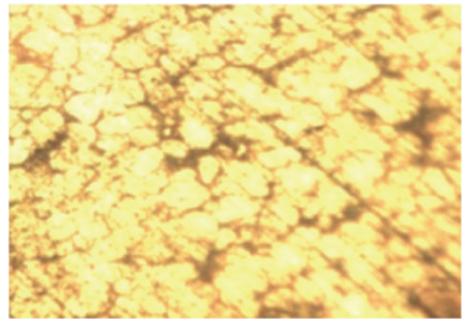

Figure 10: Microstructure of as-received scrap Al substrate (magnifications ×800).

The cast samples obtained from aluminium alloy held and poured at elevated temperature 750°C are more superheated than what was obtainable at 700°C.

Figure 11(c) shows the macrographs of aluminium cast poured at more elevated temperature (800°C) using similar sets of moulding sands as in Figures 11(a) and 11(b). At temperature as high as 800°C, there is subsequent structural change occurring in the cast aluminium alloy.

The differences in the mechanical properties (hardness, porosity, and strength) are reflection of the effects of variations in moulding sand permeability and pouring/casting temperatures on the products. Porosity may be regarded as

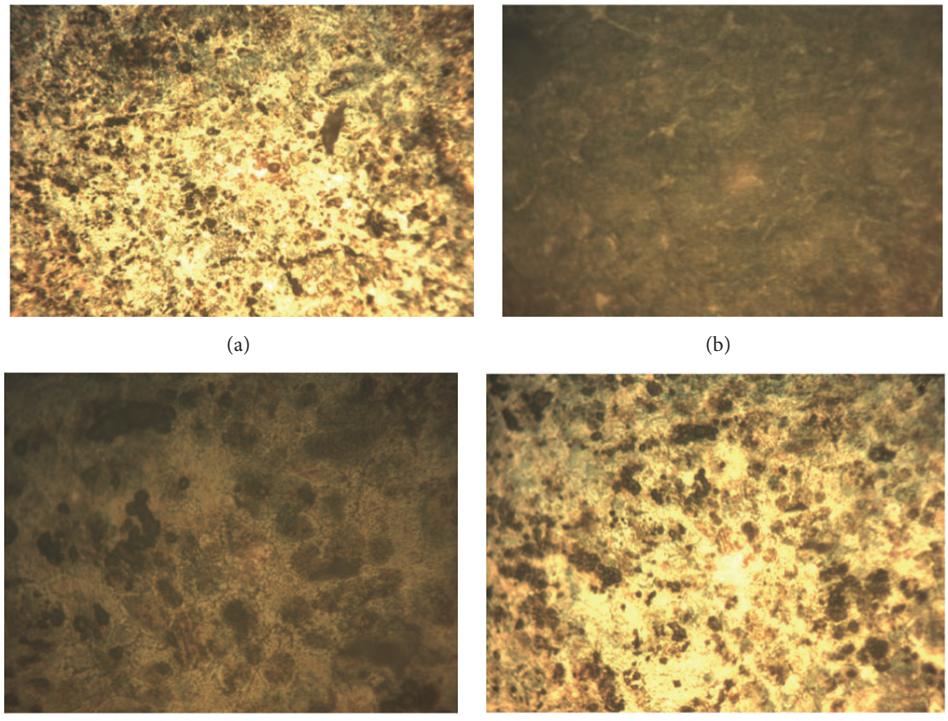

(a) (b)

(c) (d)

Figure 11: Microstructures of cast substrate poured at (a) 700 ± 10°C, (b) 750 ± 10°C, (c) 800 ± 10°C using 80 : 20, and (d) 750°C using 20 : 80 sand mixing ratios with MgFeSi (magnifications ×800).

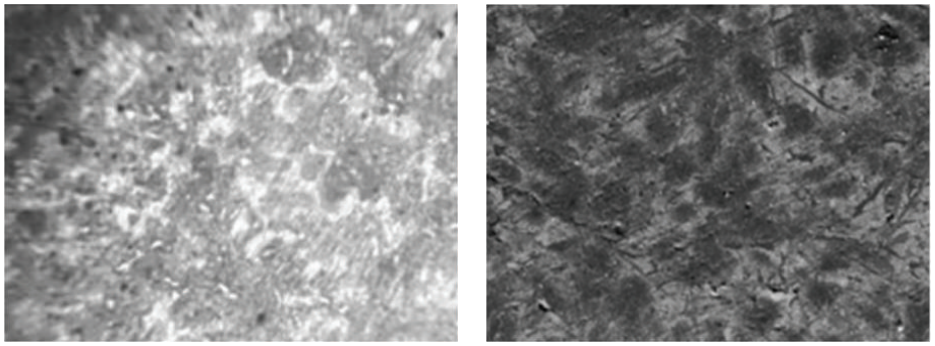

(a) (b)

Figure 12: Nucleation identified in cast alloy piston (a, b).

problem as in most casting products and in other instance being advantage in shaped porous metals. Most solid metals have higher densities than the liquid and hence the liquid metal flows in the direction of solidifying area in order to avert the formation of voids. In sand moulding, the sand permeability can be affected by the unregulated high amount of mixing water, poor compaction practice, and uneven drying which may result in the mould retaining moisture. It is much possible that when liquid metal runs across the spongy (mushy) zone to feed solidification shrinkage, the molten metal pressure in this mushy zone drops low, below the exterior atmospheric pressure. And as a result microporosity forms in the cast when the local (confined) pressure in the mushy region drops below a critical value [12].

The results of average HBN obtained from the four point hardness tests on the scrap and cast samples are presented in Figures 3(a) and 3(b). The hardness tests show that scrap sample has lower HBN than the cast piston sample. Tensile strengths of samples were determined as 154.78 Mpa for scrap sample and 226.49 Mpa for cast sample.

The addition of MgFeSi initiated nucleation in collaboration with other factors such as alloy composition, cooling rate, temperature gradient in the melt, and casting method that affect the ultimate cast grain size. With the addition of MgFeSi, the AAS characterisation shows that about 97.432% Al, 1.293% Si, 0.598% Mg, 0.202% Cu, 0.001% Zn, 0.051% Ti, 0.051% Mn, 0.041% Cr, and 0.331% Fe were contained in the cast alloy. The increase in the % Fe composition in the

Table 3: Chemical analysis of aluminium alloy samples by AAS.

Samples	Matrix	Major elements			Neutral	Microstructure modifier			Impurity
	Al	Si	Mg	Cu	Zn	Ti	Mn	Cr	Fe
Scrap Al	98.665	0.686	0.403	0.001	0.001	0.001	0.001	0.001	0.232
Cast Al	97.432	1.293	0.598	0.202	0.001	0.051	0.051	0.041	0.331

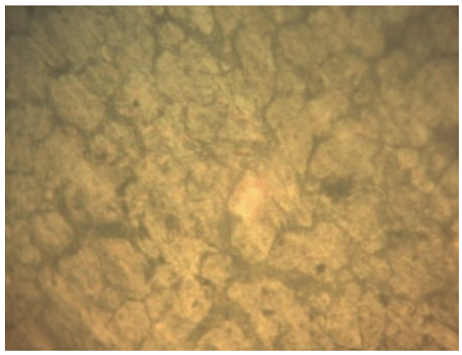

Figure 13: Microstructure of cast alloy poured at 750 ± 10°C (without inoculants) using 80 : 20 coarse-fine sand mixing ratio (magnification ×800).

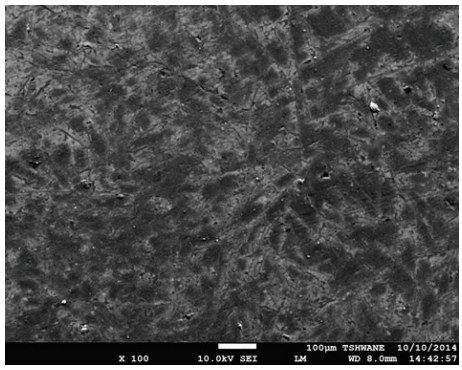

Figure 14: SEM image of 100 μm size cast alloy poured at 750 ± 10°C (with inoculant) using 80 : 20 coarse-fine sand mixing ratio (mag. ×100).

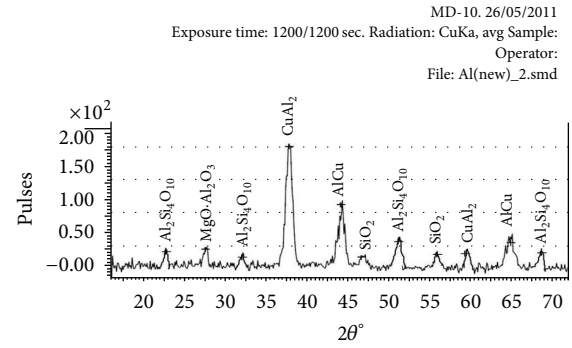

Figure 15: The diffractograms of XRD analysis of scrap sample.

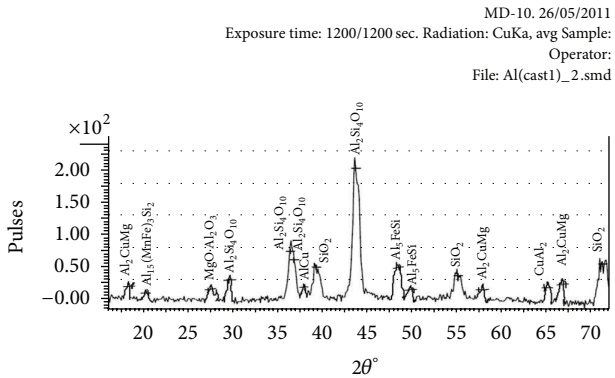

Figure 16: The diffractograms of XRD analysis of cast sample (with inoculant).

cast sample has been influenced by both the MgFeSi addition and the Fe pick-up from the melting pot. This is traced to higher solubility of Fe in molten aluminium [13]. Fine grained aluminium alloy was obtained which has better strength by inoculating the melt with MgFeSi powder which forms insoluble compound particles, thus helping to increase the rate of nucleation. In the MgFeSi modified Al-Si alloys, the growth of the Al-Si-Fe phase is cut short resulting in a large number of equiaxed Al grains formation assuming broom-resembling structures different from cast without MgFeSi [14–18] as observed in the SEM image (Figure 14).

The grain refinement of Al and its alloys using inoculants that boost heterogeneous nucleation is an important structure modification method used in many industries. A fine grain size in metal alloy castings guarantees (i) homogeneous mechanical properties, (ii) distribution of second phases and microporosity on a fine scale, (iii) superior machinability because of (ii), (iv) enhanced uniform anodizable face, (v) improved strength, toughness, and fatigue life, and (vi) superior corrosion resistance. The literature has quite a lot of mechanisms proposed for grain refinement and critical reviews exist in reports of Perhpezko [19] and McCartney [20].

In the present study, the initial scrap charge invariably contains significant amounts of iron in addition to MgFeSi inoculant, which takes an imperative function in the nucleation process. High Fe content in the charge also encourages the formation of Al-Si-Fe phase. The SEM/EDX characterisation shows that about 1.49% Si, 96.35% Al, 0.18% Cu, 0.01% Ti, 0.02% Mn, 0.02% Cr, 0.63% Fe, 0.53% Mg, and 0.01% Zn were contained in the cast alloy.

4.1.1. Variation of Pouring Temperatures and Sand Permeability on the Casting. The varying degrees of properties of cast

Table 4: SEM/EDX spectra analysis of cast alloy poured at 750 ± 10°C (with inoculant).

Sample	C	O	Si	Al	Cu	Ti	Mn	Cr	Fe	Mg	Zn
Cast Al	0.45	0.31	1.49	96.35	0.18	0.01	0.02	0.02	0.63	0.53	0.01

samples at different pouring temperatures using coarse-fine sand particle sizes mixtures are reported in Figures 3(a)–3(d).

In all cases, at any constant pouring temperature within the range of 700–800°C, the average BHN values (Figure 3(b)) and the strength (Figure 3(c)) of samples measured reduce with the reduction in sand permeability. Meanwhile, in Figure 3(d), there is increase in the trend of the cast porosity as the sand permeability reduces (Figure 3(d)). At increasing pouring temperature, the % porosity reduced with higher degree of sand permeability with respect to sand particle size ratios. The moulds made from more coarse sand have lower % porosity.

From Figures 3(a) and 3(d), it is obvious that the cast samples were characterised by quantity of moderately low % porosity (about 1.15–2.15) and moderately high % porosity (2.15–2.85), with varying sizes of both tiny pores (less than 10 μm) and large pores (above 10 μm) as observed under the microscope.

The casting voids most frequently called porosity are caused by gas formation, solidification shrinkage, or non-metallic compound formation in the molten metal. Blows or blowholes are bulky gas-related voids caused by entrapped mould or core gases in the molten metal. They are large enough and resemble bubbles with smooth internal surfaces and are buoyant and float close to the top of the casting; they can also get trapped on the bottom surface of a core lower in the mould. Moreover, pinholes are caused by gases (atoms) dissolved in molten metal (that connects and become molecules). They remain small (less than 10 μm) but float to a top surface somewhere in the casting [21].

In recent times, there are increasing interests in research on performance of castings with porosity. Most notable research is on the fracture mechanics of microplasticity models of fatigue and failure to incorporate effects of inclusions, microporosity, macroporosity, and microstructure to cast aluminium alloy components [22]. The pores are large enough to be seen even with the naked eyes on some specimen as observed in Figures 7–9. Hence, the simple evacuation approach to apparent porosity measurement was applied and the result was taken as estimate of the % apparent porosity [23]. To really calculate the fraction and size of porosity after solidification is finished, a more complex analysis may be necessary. Reports have it that the quantity and size of the porosity produced in Al-4.5 wt% Cu plate castings containing hydrogen experimentally were calculated by Kubo and Pehlke [24] while Poirier et al. [13, 25] presented such calculations for Al-Cu in directional solidification geometry.

4.2. The Surface Morphology and Porosity of Cast Aluminium Alloy Specimens. The macrographs of the surface appearances of cast aluminium alloy specimens poured at 700 ± 10, 750 ± 10, and 800 ± 10°C using four different sets of moulding sands are shown in Figures 4–6. The porosity of cast aluminium alloy obtained at different pouring temperatures and moulding sand mixing ratios are also presented in Figures 7–9.

4.3. Microstructural Examination of the Scrap and Cast Al Substrates. The microstructures obtained from the scrap and the cast Al substrates using higher resolution metallurgical microscope with digital camera under ×800 magnification are shown in Figures 10–13. The SEM image and EDX analyses of the cast sample with inoculant are presented in Figure 14 and Table 4, respectively. Figure 14 shows the SEM image of 100 μm size cast alloy poured at 750 ± 10°C (with inoculant) using 80 : 20 coarse-fine sand mixing ratio at magnification of ×100.

The images in Figures 4–6 are the photographs of the surfaces of as-cast AA6061 aluminium alloy specimens observed at ×10 magnification under High Resolution Microscopic Camera ST65-HD5X-14.2 model, while for the purpose of better clarification of the pores Figures 7–9 show the enlarged micrographs of same set of surfaces examined at ×100 magnification.

Moreover, the images in Figures 10–13 are the microstructures of 10 mm size section of the cast Al alloy examined at ×800 magnification using a metallurgical microscope, while a more magnificent image of the microstructure of a 100 μm size target was examined at ×100 magnification under the SEM (Figure 14) with the view of clarifying both the microstructure (shapes) and the elemental composition (Table 4) of the cast Al alloy specimen.

The analyses of the mechanical properties (hardness, strength) based on combination of the composition and microstructures revealed the presence of voids and inclusions in the metal cast. The primary inclusions include solids in the melt above the liquidus temperature of the alloy such as (i) the exogenous inclusions (dross, entrapped mould material, slag, and refractories); (ii) salts and fluxes suspended in the melt resulting from a previous melt-treatment processes; and (iii) suspended oxides of the melt (entrapped within by turbulence or on top of the melt). Secondary inclusions include those formed after the solidification of the main metallic phase.

4.4. Characterisation by X-Ray Diffraction Analyses of the Scrap and Cast Samples. In addition to the microphotographic examinations of the materials, the purpose of the XRD analyses in the present study is to make a distinction among the phases and the grain sizes of the microstructure with the view of appreciating and elucidating reasons for their mechanical properties (hardness and strength) and forecasting their wear behaviour.

The XRD method is based on Bragg's diffraction law [26] as follows:

$$n\lambda = 2d \sin\theta, \tag{3}$$

Table 5: XRD analysis of scrap Al sample.

S/N	Peak	Diffraction angle 2θ	Grain size (Å)	Crystal structures	Phases
1	0.20	23.0124	0.39	Triclinic	$Al_2Si_4O_{10}$
2	0.25	27.6803	0.05	Tetragonal	$MgO{\cdot}Al_2O_3$
3	0.15	32.2546	0.43	Triclinic	$Al_2Si_4O_{10}$
4	1.80	37.8674	0.14	Tetragonal	$CuAl_2$
5	0.95	46.1875	0.24	Monoclinic	AlCu
6	0.10	46.7107	0.60	Monoclinic	SiO_2
7	0.35	51.2504	0.43	Triclinic	$Al_2Si_4O_{10}$
8	0.15	56.0038	0.60	Monoclinic	SiO_2
9	0.20	59.7511	0.47	Cubic	$CuAl_2$
10	0.35	64.7793	0.10	Monoclinic	AlCu
11	0.20	68.2625	0.31	Triclinic	$Al_2Si_4O_{10}$

Table 6: XRD analysis of cast Al sample (with MgFeSi inoculant).

S/N	Peak	Diffraction angle 2θ	Grain size Å	Crystal structures	Phases
1	0.20	18.4317	0.18	Cubic	Al_2CuMg
2	0.10	20.1235	0.15	Cubic	$Al_{15}(MnFe)_3Si_2$
3	0.15	27.3567	0.15	Tetragonal	$MgO{\cdot}Al_2O_3$
4	0.03	29.5332	0.05	Triclinic	$Al_2Si_4O_{10}$
5	0.70	36.3582	0.04	Triclinic	$Al_2Si_4O_{10}$
6	2.00	36.8058	0.38	Triclinic	$Al_2Si_4O_{10}$
7	0.15	38.0476	0.10	Monoclinic	AlCu;
8	0.60	39.2411	0.60	Monoclinic	SiO_2
9	0.45	43.6492	0.34	Triclinic	$Al_2Si_4O_{10}$
10	0.50	47.1035	0.29	Cubic	Al_5FeSi
11	0.15	49.0033	0.25	Cubic	Al_5FeSi
12	0.35	55.0069	0.14	Tetragonal	SiO_4
13	0.15	56.3417	0.21	Tetragonal	Al_2CuMg
14	0.15	65.2541	0.15	Tetragonal	$CuAl_2$
15	0.15	66.7506	0.13	Cubic	Al_2CuMg
16	0.55	71.1864	0.11	Hexagonal	SiO_2

where n is the order of X-ray reflection, d is inter granular space, and λ is X-ray wavelength.

In addition to this, the average grain sizes of phases in the Al alloy samples presented in Tables 5 and 6 are determined by using Scherrer's equation [27] which is given by

$$\tau = \frac{0.9\lambda}{(\beta \cos\theta)}, \tag{4}$$

where 0.9 is the shape factor, λ is the X-ray wavelength, β is the line amplification at half of the maximum intensity (in radians), θ is Bragg's angle, and τ is the mean size of the ordered (crystalline) domains. 2θ is diffraction angle.

The grain size D is also related to the diffraction angle by

$$D = \frac{0.9\lambda}{\Delta(2\theta)\cos\theta}, \tag{5}$$

where D is the grain size and λ is the wavelength; 2θ is the diffraction angle. The parameters such as peak values, the diffraction angles, grain sizes, and the crystal structures are analysed and illustrated in Tables 5 and 6 and diffractograms (Figures 15-16). The phases of compounds at diffraction angles (2θ) and peak values which are found to be present in the samples are shown in Tables 5 and 6 and diffractograms (Figures 15-16). At a constant wavelength, the grain sizes (D) of different phase compounds are calculated from (3). Tables 5 and 6 present the XRD analyses for the scrap and cast aluminium alloy samples. By comparing the results in Tables 5 and 6, it is clear that fine grains are present more than coarse grains in the cast sample than in the as-received scrap sample. Fine grains are usually characterised by high BHN values and tensile strength properties as obtained in Figures 3(a)–3(d). Hence, there is no doubt that such cast material will possess better wear resistance property than the as-received scrap Al alloy material as compared with the previous findings [14, 16, 28]. Relatively, sets of 0.05; 0.10–0.14; 0.24; 0.31–0.39; 0.43–0.47; 0.60 Å and 0.04–0.05; 0.10–0.18; 0.21–0.29; 0.34–0.38; and 0.60 Å grain particle sizes were

obtained, respectively, for the as-received scrap and the cast samples. Higher fraction was obtained from the 0.04–0.29 Å size than the 0.34–0.60 Å sizes for cast sample.

The overall effects of variation in the pouring temperatures in combination with the moulding sand mixing ratios on the surface morphology, porosity, hardness, and strength of cast samples are illustrated Figures 3–9.

Higher casting temperature causes gassing resulting from the boiling of molten Al alloy and escape of some volatile oxides which increased the metal cast porosity hence producing porous cast with corresponding reduction in strength and hardness measured.

The best set of results were obtained from the cast specimens at 750 ± 10°C using 80 : 20 ratio of coarse and fine sand particle sizes mixture as presented in Figure 3. Under this condition, there are sufficient pores in the mould which allow the timely escape of heat, reducing the possibility of gases being entrapped in the metal cast. This explains the reasons for the wear behaviour of the cast Al alloy samples previously reported by the authors [29].

5. Conclusions

The effects of moulding sand particles mixing ratio (with respect to sand permeability) and the pouring temperatures on the hardness, porosity, and microstructures of cast aluminium pistons used in hydraulic brake master cylinder have been studied.

From the combinations of the sand mixtures made from the coarse (+4750 +300 μm) and fine (−300 −75 μm) moulding sand particle size, 80 : 20 ratio gave the best result in terms of the surface morphology. The best of the metallurgical properties such as the hardness, porosity, and microstructure were also obtained from the combination of 80 : 20 coarse-fine sand ratio and 750 ± 10°C pouring temperature. An 8 : 25 ratio of coarse-grain to fine grain eutectic aluminium alloy was obtained based on the SEM examination results. Higher BHN and strength values were also obtained by inoculating the melt with MgFeSi which forms insoluble compound particles. The SEM image of 100 μm size cast alloy poured at 750 ± 10°C shows a large number of fine Al grains formation assuming broom-resembling structures as examined in the SEM image.

Conflict of Interests

The authors declare that there is no conflict of interests regarding the publication of this paper.

Acknowledgments

The authors acknowledge the staff and management of the Premier Wings Engineering Services, Ado Ekiti, for providing the workshop services for the production and preparation of materials used for the study. Electrochemical & Materials Characterization Research Laboratory of the Tshwane University of Technology, Pretoria, South Africa, is also appreciated by the authors for the SEM analysis.

References

[1] O. O. Ajibola and B. O. Jimoh, "Aluminium recycling industries in Nigeria: entrepreneurship challenges and opportunities," in *Proceedings of the 7th Engineering Forum*, vol. 2, pp. 238–247, Ado Ekiti, Nigeria, November 2011.

[2] O. O. Ajibola, B. O. Adewuyi, and D. T. Oloruntoba, "Design and performance evaluation of wear test jig for aluminium alloy substrate in hydraulic fluid," in *Proceedings of the 8th Engineering Forum*, vol. 1, pp. 85–96, Ado Ekiti, Nigeria, October 2012.

[3] J. O. Alasoluyi, J. A. Omotoyinbo, J. O. Borode, S. O. O. Olusunle, and O. O. Adewoye, "Influence of secondary introduction of carbon and ferrosilicon on the microstructure of rotary furnace produced ductile iron," *The International Journal of Science & Technology*, vol. 2, no. 2, pp. 211–217, 2013.

[4] A. M. Hassan, A. Alrashdan, M. T. Hayajneh, and A. T. Mayyas, "Wear behavior of Al–Mg–Cu–based composites containing SiC particles," *Tribology International*, vol. 42, no. 8, pp. 1230–1238, 2009.

[5] J. E. Gruzleski and B. M. Closset, *The Treatment of Liquid Aluminium-Silicon Alloys*, AFS, Des Plaines, Ill, USA, 1st edition, 1990.

[6] P. R. Gibson, A. J. Clegg, and A. A. Das, "Wear of cast Al-Si alloys containing graphite," *Wear*, vol. 95, no. 2, pp. 193–198, 1984.

[7] P. Shanmughasundaram and R. Subramanian, "Wear behaviour of eutectic Al-Si alloy-graphite composites fabricated by combined modified two-stage stir casting and squeeze casting methods," *Advances in Materials Science and Engineering*, vol. 2013, Article ID 216536, 8 pages, 2013.

[8] S. Mahipal, B. Manjinder, S. Rohit, and A. Hitesh, "Behaviour of aluminium alloy casting with the variation of pouring temperature and permeability of sand," *International Journal of Scientific and Engineering Research*, vol. 4, no. 6, pp. 1497–1502, 2013.

[9] B. O. Jimoh, O. O. Ajibola, and S. G. Borisade, "Suitability of selected sand mine in Akure, Nigeria for use as foundry sands in aluminium alloy casting," *The International Journal of Engineering & Technology*, vol. 5, no. 8, pp. 485–495, 2015.

[10] R. J. Fruehan, "Gases in metals," in *Casting*, vol. 15 of *ASM Handbook*, ASM International, Geauga County, Ohio, USA, 9th edition, 1992.

[11] D. Apelian, *Aluminium Cast Alloy: Enabling Tools for Improved Performance*, North American Die Casting Association, Wheeling, Ill, USA, 2009.

[12] R. W. Cahn and P. Haasen, *Physical Metallurgy*, vol. 1, Elsevier, Amsterdam, The Netherlands, 4th edition, 1996.

[13] T. H. Ludwig, P. L. Schaffer, and L. Arnberg, "Influence of some trace elements on solidification path and microstructure of Al-Si foundry alloys," *Metallurgical and Materials Transactions A*, vol. 44, no. 8, pp. 3783–3796, 2013.

[14] O. O. Ajibola, D. T. Oloruntoba, and B. O. Adewuyi, "Metallurgical study of cast aluminium alloy used in hydraulic master brake calliper," *International Journal of Innovation and Scientific Research*, vol. 8, no. 2, pp. 324–333, 2014.

[15] S. Das, S. V. Prasad, and T. R. Ramachandran, "Microstructure and wear of cast (Al-Si alloy)-graphite composites," *Wear*, vol. 133, no. 1, pp. 173–187, 1989.

[16] O. O. Ajibola, B. O. Adewuyi, and D. T. Oloruntoba, "Wear behaviour of sand cast eutectic Al-Si alloy in hydraulic brake fluid," *International Journal of Innovation and Applied Studies*, vol. 6, no. 3, pp. 420–430, 2014.

[17] O. O. Ajibola, D. T. Oloruntoba, and B. O. Adewuyi, "Effects of hard surface grinding and activation on electroless-nickel plating on cast aluminium alloy substrates," *Journal of Coatings*, vol. 2014, Article ID 841619, 10 pages, 2014.

[18] O. O. Ajibola, D. T. Oloruntoba, and B. O. Adewuyi, "Design and performance evaluation of wear test jig for aluminium alloy substrate in hydraulic fluid," in *Proceedings of the Inaugural African Corrosion Congress and Exhibition (AfriCORR '14)*, Pretoria, South Africa, July 2014.

[19] J. H. Perhpezko, "Casting," in *ASM Metals Handbook*, p. 101, ASM International, Geauga County, Ohio, USA, 1988.

[20] D. G. McCartney, "Grain refining of aluminium and its alloys using inoculants," *International Materials Reviews*, vol. 34, no. 1, pp. 247–260, 1989.

[21] American Foundry Society (AFS), "Understanding porosity," in *About AFs and Metal Casting*, American Foundry Society (AFS), Schaumburg, Ill, USA, 2014, http://www.afsinc.org/.

[22] R. A. Hardin and C. Beckermann, "Effect of porosity on mechanical properties of 8630 cast steel," in *Proceedings of the 58th SFSA Technical and Operating Conference*, Paper no. 4, Steel Founders' Society of America, Chicago, Ill, USA, 2004.

[23] Determination of apparent porosity, http://www.che.iitb.ac.in/online/files/MS-207.pdf.

[24] K. Kubo and R. D. Pehlke, "Mathematical modeling of porosity formulation in solidification," *Metallurgical Transaction B*, vol. 16, pp. 359–366, 1985.

[25] D. R. Poirier, "Permeability for flow of interdendritic liquid in columnar-dendritic alloys," *Metallurgical Transaction B*, vol. 18, pp. 245–255, 1987.

[26] https://en.wikipedia.org/wiki/Bragg%27s_law, 2015.

[27] https://en.wikipedia.org/wiki/Scherrer_equation, 2015.

[28] A. B. Gurcan and T. N. Baker, "Wear behaviour of AA6061 aluminium alloy and its composites," *Wear*, vol. 188, no. 1-2, pp. 185–191, 1995.

[29] O. O. Ajibola, D. T. Oloruntoba, and B. O. Adewuyi, "Design and performance evaluation of wear test jig for aluminium alloy substrate in hydraulic fluid," *African Corrosion Journal*, vol. 1, no. 1, pp. 40–45, 2015.